ACS APPLIED ENERGY MATERIALS
Cite This: ACS Appl. Energy Mater. 2019, 2, 1259−1265
Article
www.acsaem.org

Hierarchical ZnO Microspheres Embedded in TiO_2 Photoanode for Enhanced CdS/CdSe Sensitized Solar Cells

Yuan Wang,*,† Zhou Yang,‡ Yunxia Huang,† Yangxi Yan,† Juan Hou,‖ Zhimin Li,*,† and Guozhong Cao*,†,§

†School of Advanced Materials and Nanotechnology, Xidian University, Xi'an 710126, P.R. China
‡School of Materials Science and Engineering, Shaanxi Normal University, Xi'an 710119, China
§Department of Materials and Engineering, University of Washington, Seattle, Washington 98195-2120, United States
‖Key Laboratory of Ecophysics and Department of Physics, School of Science, Shihezi University, Xinjiang 832003, P.R. China

Supporting Information

ABSTRACT: Control of structural and compositional characteristics of photoanodes is a crucial step toward rapid transport of charges and high-efficiency loading of dye or quantum dots in the case of solar cell application. Hierarchical ZnO microspheres (ZMS) and TiO_2 hybrid photoanode film were prepared for improved CdS/CdSe quantum dot sensitized solar cells (QDSCs). The addition of ZMS into TiO_2 electrode films resulted in both increased short circuit current density (J_{sc}) and open circuit voltage (V_{oc}). Such an improvement is ascribed to the increased light harvesting owing to scattering by ZMS and the reduced charge recombination due to the surface modification. TiO_2/ZMS hybrid photoanode displays superior charge injection/transport performance due to the ZMS with unique hierarchical structure, providing charge transfer continuity and multiple electron transport channels for timely electron transport. As a result, the J_{sc}, V_{oc}, and the photovoltaic conversion efficiency (PCE) were all remarkably enhanced with the insertion of hierarchical ZMS though varied appreciably with the amount of ZMS. Thus, the designed TiO_2/ZMS heterostructure-based QDSCs with an optimizing ZMS ratio of 20 wt % achieved a PCE of 5.99%, which is about 35% increase of the efficiency for the devices without ZMS (4.45%).

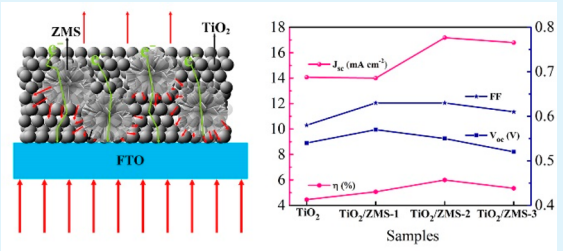

KEYWORDS: *ZnO microspheres, photoanode, light scattering, charge injection, electron transport, quantum dot-sensitized solar cells*

1. INTRODUCTION

Recently, a lot of attention has been focused on fabricating high efficient and cheap photovoltaic cells for using unlimited solar energy because of environmental damage and energy shortages.[1−4] quantum dot sensitized solar cells (QDSCs) represent a kind of promising photovoltaic devices and have attracted intensive study attribute to their low cost, easy production, and high theoretical photovoltaic conversion efficiency (PCE) (44%).[5] In recent years, considerable efforts, including novel sensitizers,[6,7] electrolytes,[8,9] counter electrodes,[10−12] photoanodes,[13,14] and also the fundamental understandings,[15] have been devoted to improve the PCE and stability of the QDSCs, and so far the record PCE grew continuously to 12.07%.[16,17]

Photoanode (porous film made of nanoparticles), as one important component in QDSCs, plays an essential role in collecting the electrons from QDs and transfers them to charge collectors.[18] It also determines the QDs' load that subsequently affects the short circuit current density (J_{sc}) of corresponding devices.[19] The porous TiO_2 film is commonly applied in QDSCs due to its high surface area for QDs' load and rich mesoporous, which facilitates the diffusion of electrolyte in/out within photoanode.[20] Nevertheless, part of the light will be lost during passing the TiO_2 electrode due to the low light scattering performance of small-sized TiO_2 nanoparticles (∼ 20 nm), resulting in the decrease of light absorption efficiency.[21] Besides, numerous interparticle boundaries and limitations in diffusion length of photoinduced carrier are involved during charge transferring within TiO_2 matrix, leading to serious recombination of electrons and holes.[22] Nevertheless, simultaneously promoting the light harness as well as photogenerated charge carrier transfer within the photoanodes are regarded as a promising method for enhancing the photovoltaic efficiency of solar cell devices.

Many efforts have focused on designing and controlling of structural and compositional characteristics of a TiO_2 electrode for improving light trapping/harvesting and facilitating the charge transfer/injection. Some methods, such as adding scattering layers on TiO_2 electrode films or TiO_2 nanoparticle-aggregates and plasmonic resonance with noble metal nanostructures have been explored for enhancing the light scattering and harvesting within the photoanode of solar

Received: October 22, 2018
Accepted: January 22, 2019
Published: January 22, 2019

DOI: 10.1021/acsaem.8b01812
ACS Appl. Energy Mater. 2019, 2, 1259−1265

cells.[23−26] The introduction of conductive nanomaterials (involving carbon nanotube and graphene) has been adopted to accelerate charge transfer in photoanode.[22,27] Recently, construction of a composite material/structure by combining the superiority of various metal oxide semiconductors as well as different nanostructures has been considered as a valid way to achieve high-efficiency QDSCs. For example, Wang et al. fabricated a composites photoanode via in situ growth of ZnO nanowires (NW) within the TiO_2 electrode using a common hydrothermal method and found that solar cells based on such photoanode were remarkably PCE enhanced by 26.9% compared to that of the devices based on pure TiO_2 nanoparticle films. This type of hybrid TiO_2/ZnO photoanode exhibits not only high light-harvesting efficiency owing to the excellent light-scattering of ZnO NW but also possesses enhanced charge transfer property arising from the one-dimensional (1D) structure.[28] Tian et al. developed a ZnO/TiO_2 nanocable photoelectrode and studied its photovoltaic performance in CdS/CdSe QDSCs.[29] Kuang et al. synthesized a three-dimensional (3D) TiO_2/ZnO hybrid array photoanode for effective QDSCs and achieved a PCE of 4.57%, which is more efficient than that of pure TiO_2 NW.[30] Wang and co-workers also prepared a hybrid photoanode with ZnO nanowires embedded in TiO_2 nanoparticles (NPs) through an in situ hydrothermal process for improved light harvesting in QDSCs. This composite architecture not only retained high surface area of pure TiO_2 photoanode film which is good for photosensitizer load but also facilitated the charge carriers collection and transport within composite electrodes by a fast lengthways transport in 1D structure.[31] In most cases, 1D ZnO nanostructures were widely assembled into the TiO_2 NPs for high -efficiency photoelectrode because they can work as a direct and fast pathway for photoinduced charge to transfer along the axis direction of 1D, and the electron mobility of ZnO is about 4 times higher than that of TiO_2. However, such 1D nanostructures possess low surface area for QDs loading as well as limited light scattering effect, and consequently result in insufficient light utilization as well as photovoltaic efficiency. In recent years, the 3D hierarchical ZnO microspheres (ZMS) consisting of high-specific-surface-area nanosheets are said to be good for utilizing light due to the excellent light-scattering ability resulted from their open 3D strucure, electron transport property due to the secondary two dimension (2D) structure, and large surface area provided by nanosheets.[32] The hierarchical ZMS instead of 1D ZnO will likely produce enhanced photovoltaic performance for TiO_2 NPs-based photoanode in QDSCs.

In the present study, 3D hierarchical ZMS is constructed through a facile and surfactant-free chemical solution route and incorporated into TiO_2 photoanodes. The 3D ZMS frameworks with micron-sized structure consisted of packed nanosheets serve as the light scattering centers and provide effective charge transfer channels, as shown in Scheme 1. In order to determine the optimum ZMS packing mass ratio, bare TiO_2 as well as a series of TiO_2/ZMS (10%, 20%, and 30.0%) were studied to form photoanodes of QDSCs. The results showed that QDSCs with TiO_2/ZMS heterostructure with ZMS ratio of 20 wt % achieved a PCE of 5.99%, 35% higher than devices based on TiO_2 NPs photoanode. The effects of ZMS on light scattering and charge transfer through the photoanodes were studied via diffused reflectance spectra, the photoluminescence spectra, decay curves, and electrochemical impedance spectroscopy to demonstrate the effect of ZMS content on the photovoltaic performance of hybrid ZMS/TiO_2 based QDSCs.

Scheme 1. Schematic Picture of Electron (e^-) Diffuse and Sunlight Passing Pathway[a]

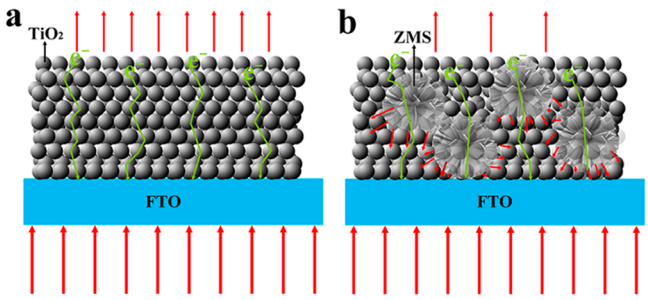

[a]Within (a) TiO_2 and (b) TiO_2/ZMS matrix.

2. EXPERIMENTAL SECTION

2.1. Fabrication of TiO_2/ZMS Heterostructure Films. To synthesize TiO_2/ZMS heterostructural electrode films, hierarchical ZMS was first prepared by our previous reported procedure.[32] For fabrication of the mesoporous TiO_2/ZMS electrodes, the TiO_2 (Degussa P25, Aladdin) with different ZMS ratios (TiO_2/ZMS mass ratio of 0%, 10%, 20%, and 30%), ethyl cellulose, and terpineol were blended together to form a paste. Then the obtained paste was manually scrape-coated on fluorine-doped tin oxide (2.2 mm, 14 Ω) glass and calcining at 500 °C for 30 min for improved crystallization and removing organic matter afterward. The thickness of the obtained hybrid film estimated by SEM picture was ∼14 ± 1 μm.

2.2. Preparation of CdS/CdSe Cosensitized Photoanode and Device Assembly. Above fabricated TiO_2/ZMS hybrid film were successively sensitized by depositing CdS and CdSe QDs and subsequently deposited with a ZnS passivation layer. The obtained photoanode together with Cu counter electrode and polysulfide electrolyte form a sandwich lamination structured device. Refer to our previous literature for the detail process.[33]

2.3. Materials and Device Characterization. The top and cross-section views of prepared TiO_2/ZMS heterostructure photoelectrode was observed using scanning electron microscope (SEM, JSM-7000) as well as transmission electron microscope (TEM, Tecnai G2 F20) microscopy. All X-ray diffraction (XRD, Rigaku-Dmax 2500) patterns were performed by Cu Kα radiation (λ = 0.15405 nm, 40 kV, 30 mA). The energy-dispersive spectroscopy (EDS) and EDS mapping images were obtained by an X-ray energy dispersive spectrometer combined with above-mentioned SEM installation. The absorption capacity of different films was analyzed by the optical absorption (Lambda 950, PerkinElmer). Furthermore, the photoluminescence (PL) spectra as well as PL decay curves were estimated by a fluorescence spectrometer (Edinburgh Instruments FLS920). The photoelectric performance was tested by a HP 4155A workstation. The incident photon-to-current conversion efficiency (IPCE, 7-SCSpec response system) was used to analyze the electron injection and charge carries lifetime within different devices. Electrochemical impedance spectroscopy (EIS, Solartron 1260 FRA/impedance analyzer) was performed to further study charge transfer resistant in devices.

3. RESULTS AND DISCUSSION

Figure 1 displays SEM images of the hierarchical ZMS and top view of the TiO_2/ZMS films. The ZMS is an open 3D sphere and the diameters are about 2∼4 μm (Figure 1a). The magnified SEM (Figure 1b) displays that each microsphere was assembled from packed nanosheets with rough surface and ∼20 nm thickness. The typical top-view SEM images of TiO_2/ZMS films fabricated by coating various mass ratio of TiO_2 and

DOI: 10.1021/acsaem.8b01812
ACS Appl. Energy Mater. 2019, 2, 1259−1265

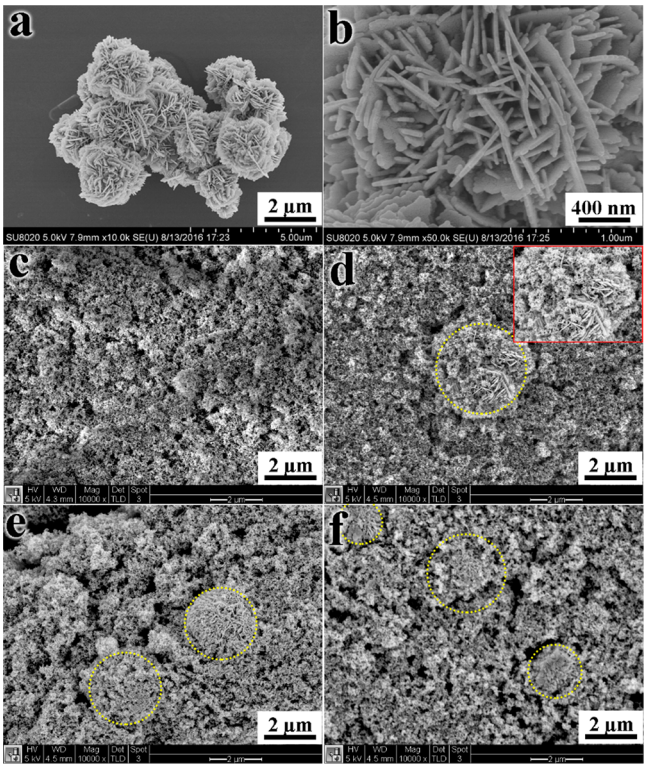

Figure 1. SEM and high-magnification images of (a,b) ZMS. Top view SEM pictures of (c) TiO_2, (d) TiO_2/ZMS-1, (e) TiO_2/ZMS-2, and (f) TiO_2/ZMS-3 photoanode films.

ZMS mixed paste are exhibited in Figure 1c–f and the ratio of ZMS and TiO_2 films are 0 (c), 10 (d), 20 (e), and 30 wt % (f), respectively. Figure 1d and the inset in Figure 1d shows that only a few hierarchical ZMS well- embedded in the film and the structural features of the ZMS remain unchanged and surrounded by the TiO_2 NPs. As the ratio increased to 20 and 30 wt %, there is a gradual increase in the density of ZMS. Figure 2 shows XRD patterns of the TiO_2/ZMS hybrid films

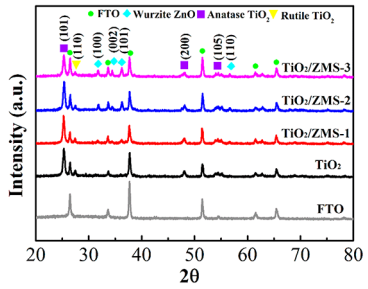

Figure 2. XRD patterns of TiO_2, TiO_2/ZMS-1, TiO_2/ZMS-2, and TiO_2/ZMS-3 films.

and pure TiO_2 film on FTO substrates. All diffraction peaks of TiO_2/ZMS films are good in agreement with hexagonal wurzite ZnO, anatase TiO_2, and rutile TiO_2.[28,34,35] Obviously, when increasing the ratio of ZMS, intensities of ZnO peaks (100), (002), (110), and (101) enhance gradually.

The diffused reflectance spectra of TiO_2/ZMS hybrid films and pure TiO_2 film were performed, as shown in Figure 3. Apparently, TiO_2/ZMS hybrid films possessed higher reflection intensity in the wavelength ranging from 380 to 800 nm than bare TiO_2 film. Note that the reflectivity of the

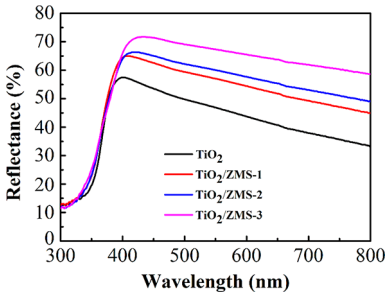

Figure 3. Diffuse reflectance spectra of the TiO_2, TiO_2/ZMS-1, TiO_2/ZMS-2, and TiO_2/ZMS-3 films.

TiO_2/ZMS heterostructures increases steadily with the increased amount of ZMS, indicating this randomly distributed ZMS led to the higher light harvesting of the photoanodes, confirming the light scattering effect of the ZMS within the TiO_2 NPs film.[28,36]

From the cross-sectional view of TiO_2/ZMS-2 mesoporous film with CdS/CdSe QDs and ZnS passivation layer shown in Figure 4a, the thickness is measured to be about 14 μm. The

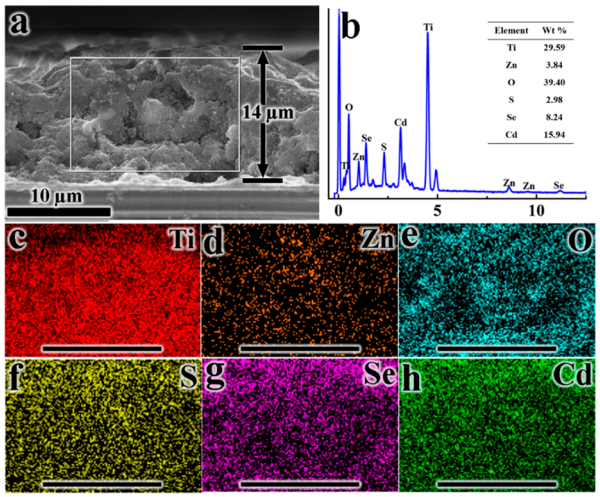

Figure 4. (a) Cross-sectional view, (b) EDS, and (c–h) EDS mapping of rectangular region.

EDS and EDS mapping (Figure 4b–h) of all elements in the TiO_2/ZMS-2-based photoanodes were studied by selecting a rectangular region in cross-section, as shown in Figure 4a. As shown in Figure 5b, we can easily observe the peaks for Ti, Zn, O, S, Se, and Cd with mass ratios of 29.6:3.8:39.4:3.0:8.2:15.9 in the photoanode. More importantly, all elements involving in this film uniform distribution throughout the whole film (Figure 4c–h).

Figure 5a shows optical absorption spectra of TiO_2/ZMS/CdS/CdSe electrodes with various ZMS ratios over the wavelengths from 350 to 800 nm. Apparently, compared with photoanode film without ZMS, the photoanodes with ZMS exhibit not only an enhancement in the absorbance intensity but also a slight extension in absorption range. The high absorbance of the hybrid TiO_2/ZMS/CdS/CdSe films indicates that more CdS and CdSe QDs were successfully loaded.[37] Note that there is a strong dependence on ZMS mass ratios for the absorbance of the TiO_2/ZMS hybrid films. The loading amount of QDs would increase with increasing the ZMS, leading to an enhance in the absorbance.

DOI: 10.1021/acsaem.8b01812
ACS Appl. Energy Mater. 2019, 2, 1259–1265

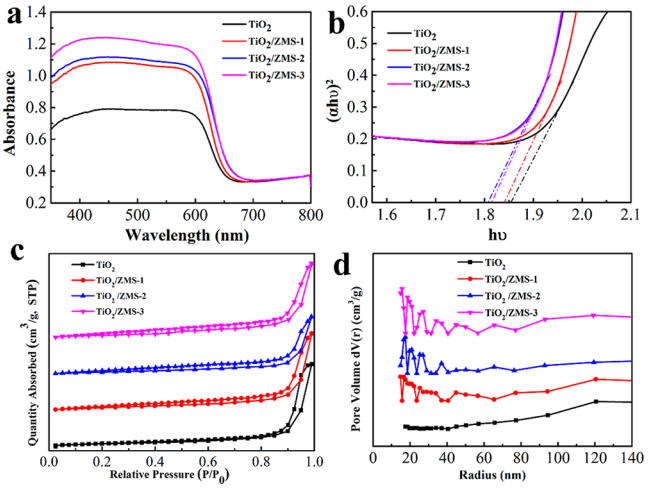

Figure 5. (a) UV−visible absorption spectra, (b) $(A h\nu)^2$ versus $h\nu$ curves, (c) nitrogen adsorption and desorption isotherms, and (d) pore-size with gas desorption distribution of of TiO_2/ZMS/QDs based photoanodes with various contents of ZMS.

As shown in Figure 5b, the QDs bandgap was evaluated by linear section of $(A h\nu)^2$ against $h\nu$ curve using extrapolation method.[38,39] Apparently, the TiO_2/ZMS/CdS/CdSe photoanode displays higher light-harvesting ability than that of the photoanode without hierarchical ZMS, in turn, this facilitates the enhancement in the photovoltaic performance of photoanode. The surface areas as well as pore size distributions of TiO_2 and TiO_2/ZMS are also investigated by nitrogen sorption isotherms (Figure 5c,d), which are employed to further analyze whether the increased light harvesting comes from changes of specific surface area. The BET results show a distinct hysteresis loop between 0.8 and 1.0 with high relative pressures in all isotherms (Figure 5c), indicating that the mesoporous structures inside the TiO_2 films is preserved after introducing of ZMS. Figure 5d shows that smaller mesoporous (15−30 nm) was observed in TiO_2/ZMS based photoanodes, which apparently originates from hierarchical ZnO microspheres itself. Note that the surface area gradually decreased from 66.2 m^2/g (TiO_2) to 65.3 m^2/g (TiO_2/ZMS-1), 56.1 m^2/g (TiO_2/ZMS-2), and 50.5 m^2/g (TiO_2/ZMS-3) with increasing ZMS ration because of larger-sized ZMS with open structure. In this sense, the enhanced light harvesting possibly derived from plenty of microspore structure and exposed rough nanosheet surface (as evidenced by Figure 1b) of the hierarchical ZMS for more QDs loading. On the other hand, the slight red shift of the onset absorption with increasing ZMS is ascribed to size quantization effects of involved QDs as reported in the literature.[40,41]

The $J-V$ curves of all prepared solar cells with area of 0.16 cm^2 were performed using standard simulated sunlight (AM 1.5G at 100 mW cm^{-2}), as shown in Figure 6a. Table 1 gives the performance parameters of various devices and Figure 6b demonstrates the changing trend J_{sc}, V_{oc}, F,F and η. When bare TiO_2 film loaded with CdS/CdSe, the J_{sc}, V_{oc}, FF, and η of the device were 14.07 mA cm^{-2}, 0.58 V, 0.54, and 4.45%, respectively. After embedding hierarchical ZMS into TiO_2 NPs film, the η of the CdS/CdSe cosensitized device increases markedly with 5.06% for TiO_2/ZMS-1 and 5.99% for TiO_2/ZMS-2, respectively. Afterward, by continuing increasing the ZMS mass ratio to 30%, η reduces to 5.34%. This result can be explained that the incorporation of hierarchical ZMS would

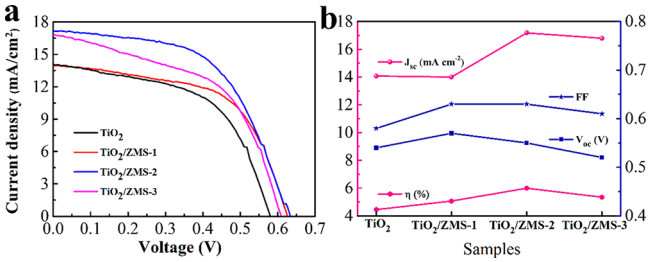

Figure 6. (a) $J-V$ curves of TiO_2/ZMS-based QDSCs with different contents of ZMS and (b) change trends of V_{oc}, J_{sc}, FF, and η with increase the amount of ZMS.

Table 1. Corresponding Photovoltaic Parameters Calculated from $J-V$ Results for Different TiO_2/ZMS Based Devices

samples	V_{oc} (V)	J_{sc} (mA cm^{-2})	FF	η (%)
TiO_2	0.58	14.07	0.54	4.45
TiO_2/ZMS-1	0.63	14.00	0.57	5.06
TiO_2/ZMS-2	0.63	17.18	0.55	5.99
TiO_2/ZMS-3	0.61	16.79	0.52	5.34

promote the electron transport and lower charge recombination from the unique hierarchical architecture; however, too much ZMS would increase the charge recombination occurring during electrons passing from ZnO to oxidized ions in the electrolyte, resulting in a deteriorated FF and V_{oc} of a solar cell, finally leading to the device performance decrease in the case of TiO_2/ZMS-3. The IPCE of the prepared devices with various ZMS against wavelength are displayed in Figure S1 and corresponding calculated J_{sc} for TiO_2, TiO_2/ZMS-1, TiO_2/ZMS-2, and TiO_2/ZMS-3 based QDSCs are 12.39, 12.44, 15.68, and 14.93 mA cm^{-2}, respectively, which are consistent with measured trend (Figure 6a).

We also studied EIS to further conform the influence of the ZMS on the electron transfer of the QDSCs. Figure 7a presents the Nyquist plots measured from various TiO_2/ZMS based cells. Table 2 gives all the fitting results fitted using the equivalent circuit (inset Figure 7a). It could be observed that all samples have two semicircles connected with the electro-

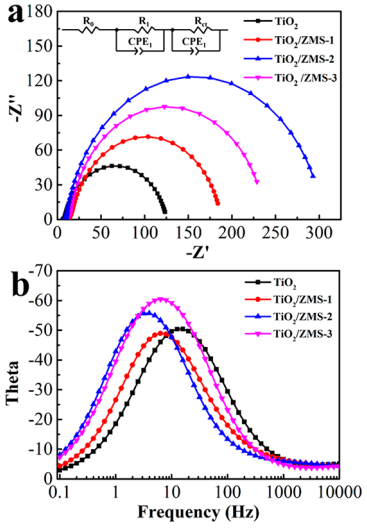

Figure 7. (a) Nyquist plots and (b) bode plots of TiO_2/ZMS based QDSCs with different contents of ZMS.

DOI: 10.1021/acsaem.8b01812
ACS Appl. Energy Mater. 2019, 2, 1259−1265

Table 2. Fitting and Calculated Results from Nyquist Plots and Bode Plots of TiO_2/ZMS-based QDSCs with Various Contents of ZMS

samples	R_{ct} (Ω)	τ_n (ms)
TiO_2	117.2	12.7
TiO_2/ZMS-1	168.8	25.2
TiO_2/ZMS-2	294.9	40.0
TiO_2/ZMS-3	224.0	25.3

chemical resistance in counter electrode (R_1) and charge transport resistance (R_{ct}) in the photoelectrode.[42−44] No obvious change was observed in R_1 among various devices because each cell is assembled with same counter electrode as well as electrolyte. Generally, the R_{ct} demonstrated via radius of the large semicircle indicates charge recombination efficiency within photoanode and a large R_{ct} value stands for a low charge recombination rate. We can see that the R_{ct} of the device with pure TiO_2 photoanode is only 117.2 Ω, while the R_{ct} for the TiO_2/ZMS-1 and TiO_2/ZMS-2 based QDSCs reached 168.8 and 294.9, respectively. Furthermore, the R_{ct} value reduced when continuing to add more ZMS, showing the same trend with $J-V$ data. These results further demonstrate that electron transfer efficiency was significantly improved by being incorporated with a certain amount of ZMS. Figure 7b displays corresponding bode plots and electron lifetime (τ_n) are evaluated using following equation[37,38]

$$\tau_n = \frac{1}{\omega_{min}} = \frac{1}{2\pi f_{min}}$$

The calculated τ_n value of the QDSCs with 20% ZMS (40.0 ms) is much higher than the device without ZMS (12.7 ms) (Table 2). The improvement in R_{ct} as well as τ_n further suggests an increased charge transfer efficiency in interface of the TiO_2/ZMS/QDs/electrolyte and provides strong evidence for the higher V_{oc} of TiO_2/ZMS-based QDSCs.

Steady-state photoluminescence (PL) spectra were performed under an excitation wavelength of 370 nm to investigate the trap states of CdS and CdSe QDs and charge injection from QDs to the electron transport layer. As shown in Figure 8a, there are two broad emission peaks in the range of 440−480 nm and a noticeable peak at ∼635 nm. The broad peaks centered in the range of 440−480 nm can be attributed to oxygen vacancies within TiO_2 and ZMS, and low emission intensity of the TiO_2/ZMS-based photoanode proves that the amount of surface defects is reduced.[39,45] The remarkable reduction in these two emission peaks of TiO_2/ZMS-based photoanode with adding ZMS mass ratio further demonstrates a reduced photogenerated carries recombination in photoanode arising from the unique hierarchical structure of ZMS and lower surface defects caused by decreased surface area. The strong peak at 635 nm can be ascribed to excitonic emission of CdSe QDs, as magnification shows in Figure 8b.[46] The PL emission of the QDs is apparently inhibited by introduction of ZMS with an increased amount of ZMS, as compared to the TiO_2 photoanode. These results combine with optical absorption data demonstrated a more efficient electron injection occurring within TiO_2/ZMS/CdS/CdSe interface, likely due to the ZMS with hierarchical architecture may provide multichannel for timely electron transport.[47] Notably, when the ZMS content is increased to 30 wt %, the PL intensity slightly increases, suggesting the same trend with the EIS and PCE. In view of the above results, it is evident that

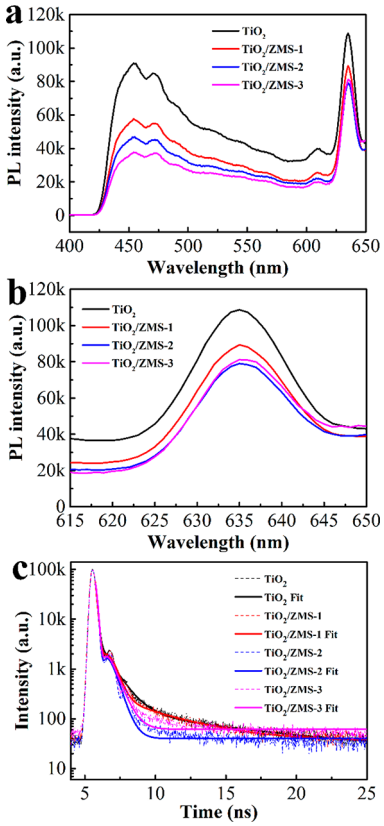

Figure 8. (a,b) PL and (c) normalized PL decay curves of TiO_2/ZMS/QDs photoanodes with various contents of ZMS.

incorporation of ZMS within TiO_2 photoanode simultaneously accelerates the electron injection to TiO_2 and prohibits recombination of photoinduced charge within the photoelectrode.

The corresponding PL decay curves of all prepared photoelectrodes are displayed in Figure 8c. The average PL lifetime of the TiO_2/QDs is 1.17 ns, and it decreases to 0.73 and 0.29 when the ZMS content is gradually increased to 10 and 20 wt %, respectively. Afterward, to continue to increase ZMS to 30 wt %, the average lifetimes increase slightly to 0.33 ns. The reduced PL decay lifetime indicates more efficient extraction and transport at the interface of TiO_2/ZMS-based photoelectrode than in the pure TiO_2 based film.[33,48,49] This result combined with EIS and PL data indicates that excellent photovoltaic performance of TiO_2/ZMS devices is also derived from both high electron transport and electron injection efficiency.

Scheme 1 illustrates the sunlight transmission as well as electron diffusion pathway in a pure TiO_2 NPs and TiO_2/ZMS heterostructured photoanode, respectively. The ZMS embedded within TiO_2 photoanode plays significant roles in improving light scattering as well as enhancing electron collection, as evidenced by above diffused reflectance spectra, EIS and PL results. And the ZMS with both 3D microspore structure and 2D rough exposed nanosheet facilitates rapid transport of charges and more loading of QDs within the film matrix. In TiO_2 photoanode, most of the light passing through TiO_2 films will loss due to the low light scattering of small-sized TiO_2 NPs, resulting in the decrease of the light harvesting efficiency. Scheme 1b reveals that parts of the unabsorbed light waves within the TiO_2/ZMS photoelectrode are iteratively

DOI: 10.1021/acsaem.8b01812
ACS Appl. Energy Mater. 2019, 2, 1259−1265

stopped by rounded ZMS and experienced a secondary utilization. Meanwhile, such a hierarchical ZnO microspheres structure can work as a direct channel for fast charge transport photoanode films. Thus, fabrication of TiO_2/ZMS hybrid photoanode has proved to be an efficient method to improve charge transfer and injection as well as light harvesting.

4. CONCLUSIONS

TiO_2/ZMS photoanodes with hierarchical ZMS homogeneously incorporated in TiO_2 matrix are prepared as working electrode for constructing high efficiency CdS/CdSe cosensitized QDSCs. This TiO_2/ZMS hybrid architecture displays advantages mainly in the J_{sc} and V_{oc} primarily ascribed to the scattering centers of light for repeating reflection of light waves within photoelectrode and lower charge recombination arising from fast multichannel for electron transport though the unique ZMS structure. The EIS, PL, and PL decay results further confirm that that the TiO_2/ZMS hybrid electrodes exhibit more excellent electron transfer and injection ability as compared with pure TiO_2 electrode. Taking all the factors into account, we may safely conclude that the fabricated TiO_2/ZMS heterostructure-based QDSCs exhibit continuous enhancement in J_{sc}, V_{oc} and the corresponding η as increasing the ZMS mass ratio from 0 wt % to 20 wt %. It is found that 20 wt % TiO_2/ZMS cell achieved the maximum efficiency (5.99%) among a series of ZMS packing ratios of 0%, 10%, 20%, and 30.0%, which is about 35% enhanced for the devices without ZMS (4.45%). When ZMS ratio was further increased to 30 wt %, the PCE decreased slightly to 5.34%, which presents the same trend with the EIS as well as PL decay lifetime data.

■ ASSOCIATED CONTENT

Supporting Information

The Supporting Information is available free of charge on the ACS Publications website at DOI: 10.1021/acsaem.8b01812.

IPCE curves of prepared films (PDF)

■ AUTHOR INFORMATION

Corresponding Authors

*E-mail: yuanwang@xidian.edu.cn (Y.W.).
*E-mail: zmli@mail.xidian.edu.cn (Z.L.).
*E-mail: gzcao@u.washington.edu (G.C.).

ORCID

Guozhong Cao: 0000-0001-6539-0490

Notes

The authors declare no competing financial interest.

■ ACKNOWLEDGMENTS

Authors would like to acknowledge the financial supports of the National Natural Science Foundation of China (Nos. 61804115, 51602240, and 61704114), Natural Science Basic Research Plan in Shaanxi Province of China (2018JQ5007, 2018JM5060, and 2017JQ5112) and the Fundamental Research Funds for the Central Universities (No. JBX171413).

■ REFERENCES

(1) Ye, M.; Gao, X.; Hong, X.; Liu, Q.; He, C.; Liu, X.; Lin, C. Recent Advances in Quantum Dot-sensitized Solar Cells: Insights into Photoanodes, Sensitizers, Electrolytes and Counter Electrodes. *Sust. Energy Fuels* **2017**, *1*, 1217−1231.

(2) Rauf, I. A.; Rezai, P. A Review of Materials Selection for Optimized Efficiency in Quantum Dot Sensitized Solar Cells: A Simplified Approach to Reviewing Literature Data. *Renewable Sustainable Energy Rev.* **2017**, *73*, 408−422.

(3) Huang, F.; Hou, J.; Wang, H.; Tang, H.; Liu, Z.; Zhang, L.; Zhang, Q.; Peng, S.; Liu, J.; Cao, G. Impacts of Surface or Interface Chemistry of ZnSe Passivation Layer on the Performance of CdS/CdSe Quantum Dot Sensitized Solar Cells. *Nano Energy* **2017**, *32*, 433−440.

(4) Wu, W.; Haick, H. Materials and Wearable Devices for Autonomous Monitoring of Physiological Markers. *Adv. Mater.* **2018**, *30*, 1705024.

(5) Sun, J.-K.; Jiang, Y.; Zhong, X.; Hu, J.-S.; Wan, L.-J. Three-Dimensional Nanostructured Electrodes for Efficient Quantum-Dot-Sensitized Solar Cells. *Nano Energy* **2017**, *32*, 130−156.

(6) Wang, J.; Li, Y.; Shen, Q.; Izuishi, T.; Pan, Z.; Zhao, K.; Zhong, X. Mn Doped Quantum Dot Sensitized Solar Cells with Power Conversion Efficiency Exceeding 9%. *J. Mater. Chem. A* **2016**, *4*, 877−886.

(7) Du, J.; Du, Z.; Hu, J.-S.; Pan, Z.; Shen, Q.; Sun, J.; Long, D.; Dong, H.; Sun, L.; Zhong, X.; et al. Zn−Cu−In−Se Quantum Dot Solar Cells with a Certified Power Conversion Efficiency of 11.6%. *J. Am. Chem. Soc.* **2016**, *138*, 4201−4209.

(8) Feng, W.; Li, Y.; Du, J.; Wang, W.; Zhong, X. Highly Efficient and Stable Quasi-Solid-State Quantum Dot-Sensitized Solar Cells Based on a Superabsorbent Polyelectrolyte. *J. Mater. Chem. A* **2016**, *4*, 1461−1468.

(9) Tian, J.; Shen, T.; Liu, X.; Fei, C.; Lv, L.; Cao, G.; et al. Enhanced Performance of PbS-Quantum-Dot-Sensitized Solar Cells via Optimizing Precursor Solution and Electrolytes. *Sci. Rep.* **2016**, *6*, 23094.

(10) Du, Z.; Pan, Z.; Fabregat-Santiago, F.; Zhao, K.; Long, D.; Zhang, H.; Zhao, Y.; Zhong, X.; Yu, J.-S.; Bisquert, J. Carbon Counter-Electrode-Based Quantum-Dot-Sensitized Solar Cells with Certified Efficiency Exceeding 11%. *J. Phys. Chem. Lett.* **2016**, *7*, 3103−3111.

(11) Kim, H.-J.; Ko, B.; Gopi, C. V.; Venkata-Haritha, M.; Lee, Y.-S. Facile Synthesis of Morphology Dependent CuS Nanoparticle Thin Film as a Highly Efficient Counter Electrode for Quantum Dot-Sensitized Solar cells. *J. Electroanal. Chem.* **2017**, *791*, 95−102.

(12) Zhang, H.; Wang, C.; Peng, W.; Yang, C.; Zhong, X. Quantum Dot Sensitized Solar Cells with Efficiency up to 8.7% Based on Heavily Copper-Deficient Copper Selenide Counter Electrode. *Nano Energy* **2016**, *23*, 60−69.

(13) Prasad, M. R.; Kadam, V.; Joo, O.-S.; Pathan, H. M.; et al. Improving the Photovoltaic Parameters in Quantum Dot Sensitized Solar Cells Through Employment of Chemically Deposited Compact Titania Blocking Layer. *Mater. Chem. Phys.* **2017**, *194*, 165−171.

(14) Shen, T.; Tian, J.; Li, B.; Cao, G. Ultrathin ALD Coating on TiO_2 Photoanodes with Enhanced Quantum Dot Loading and Charge Collection in Quantum Dots Sensitized Solar Cells. *Sci. China Mater.* **2016**, *59*, 833−841.

(15) Tian, J.; Cao, G. Design, Fabrication and Modification of Metal Oxide Semiconductor for Improving Conversion Efficiency of Excitonic Solar Cells. *Coord. Chem. Rev.* **2016**, *320*, 193−215.

(16) Mathew, S.; Yella, A.; Gao, P.; Humphry-Baker, R.; Curchod, B. F.; Ashari-Astani, N.; Tavernelli, I.; Rothlisberger, U.; Nazeeruddin, M. K.; Grätzel, M. Dye-Sensitized Solar Cells with 13% Efficiency Achieved Through the Molecular Engineering of Porphyrin Sensitizers. *Nat. Chem.* **2014**, *6*, 242−247.

(17) Jiao, S.; Du, J.; Du, Z.; Long, D.; Jiang, W.; Pan, Z.; Li, Y.; Zhong, X. Nitrogen-Doped Mesoporous Carbons as Counter Electrodes in Quantum Dot Sensitized Solar Cells with a Conversion Efficiency Exceeding 12%. *J. Phys. Chem. Lett.* **2017**, *8*, 559−564.

(18) Zhang, Q.; Guo, X.; Huang, X.; Huang, S.; Li, D.; Luo, Y.; Shen, Q.; Toyoda, T.; Meng, Q. Highly Efficient CdS/CdSe-Sensitized Solar Cells Controlled by the Structural Properties of Compact Porous TiO_2 Photoelectrodes. *Phys. Chem. Chem. Phys.* **2011**, *13*, 4659−4667.

DOI: 10.1021/acsaem.8b01812
ACS Appl. Energy Mater. 2019, 2, 1259−1265

(19) Tian, J.; Cao, G. Control of Nanostructures and Interfaces of Metal Oxide Semiconductors for Quantum-Dots-Sensitized Solar Cells. *J. Phys. Chem. Lett.* **2015**, *6*, 1859−1869.
(20) Xu, Y.-F.; Wu, W.-Q.; Rao, H.-S.; Chen, H.-Y.; Kuang, D.-B.; Su, C.-Y. CdS/CdSe Co-Sensitized TiO_2 Nanowire-Coated Hollow Spheres Exceeding 6% Photovoltaic Performance. *Nano Energy* **2015**, *11*, 621−630.
(21) Ye, M.; Zheng, D.; Lv, M.; Chen, C.; Lin, C.; Lin, Z. Hierarchically Structured Nanotubes for Highly Efficient Dye-Sensitized Solar Cells. *Adv. Mater.* **2013**, *25*, 3039−3044.
(22) Zhu, Y.; Meng, X.; Cui, H.; Jia, S.; Dong, J.; Zheng, J.; Zhao, J.; Wang, Z.; Li, L.; Zhang, L.; et al. Graphene Frameworks Promoted Electron Transport in Quantum Dot-Sensitized Solar Cells. *ACS Appl. Mater. Interfaces* **2014**, *6*, 13833−13840.
(23) Zhao, H.; Huang, F.; Hou, J.; Liu, Z.; Wu, Q.; Cao, H.; Jing, Q.; Peng, S.; Cao, G. Efficiency Enhancement of Quantum Dot Sensitized TiO_2/ZnO Nanorod Arrays Solar Cells by Plasmonic Ag Nanoparticles. *ACS Appl. Mater. Interfaces* **2016**, *8*, 26675−26682.
(24) Wang, H.; Miyauchi, M.; Ishikawa, Y.; Pyatenko, A.; Koshizaki, N.; Li, Y.; Li, L.; Li, X.; Bando, Y.; Golberg, D. Single-Crystalline Rutile TiO_2 Hollow Spheres: Room-Temperature Synthesis, Tailored Visible-Light-Extinction, and Effective Scattering Layer for Quantum Dot-Sensitized Solar Cells. *J. Am. Chem. Soc.* **2011**, *133*, 19102−19109.
(25) Han, S. H.; Lee, S.; Shin, H.; Suk Jung, H. A Quasi-Inverse Opal Layer Based on Highly Crystalline TiO_2 Nanoparticles: A New Light-Scattering Layer in Dye-Sensitized Solar Cells. *Adv. Energy. Mater.* **2011**, *1*, 546−550.
(26) Wooh, S.; Yoon, H.; Jung, J. H.; Lee, Y. G.; Koh, J. H.; Lee, B.; Kang, Y. S.; Char, K. Efficient Light Harvesting with Micropatterned 3D Pyramidal Photoanodes in Dye-Sensitized Solar Cells. *Adv. Mater.* **2013**, *25*, 3111−3116.
(27) Chen, J.; Li, B.; Zheng, J.; Zhao, J.; Zhu, Z. Role of Carbon Nanotubes in Dye-Sensitized TiO_2-Based Solar Cells. *J. Phys. Chem. C* **2012**, *116*, 14848−14856.
(28) Bai, Y.; Yu, H.; Li, Z.; Amal, R.; Lu, G. Q. M.; Wang, L. In Situ Growth of a ZnO Nanowire Network within a TiO_2 Nanoparticle Film for Enhanced Dye-Sensitized Solar Cell Performance. *Adv. Mater.* **2012**, *24*, 5850−5856.
(29) Tian, J.; Zhang, Q.; Zhang, L.; Gao, R.; Shen, L.; Zhang, S.; Qu, X.; Cao, G. ZnO/TiO_2 Nanocable Structured Photoelectrodes for CdS/CdSe Quantum Dot Co-Sensitized Solar Cells. *Nanoscale* **2013**, *5*, 936−943.
(30) Feng, H.-L.; Wu, W.-Q.; Rao, H.-S.; Wan, Q.; Li, L.-B.; Kuang, D.-B.; Su, C.-Y. Three-Dimensional TiO_2/ZnO Hybrid Array as a Heterostructured Anode for Efficient Quantum-Dot-Sensitized Solar Cells. *ACS Appl. Mater. Interfaces* **2015**, *7*, 5199−5205.
(31) Deng, J.; Wang, M.; Zhang, P.; Ye, W. Preparing ZnO Nanowires in Mesoporous TiO_2 Photoanode by an in-situ Hydrothermal Growth for Enhanced Light-Trapping in Quantum Dots-Sensitized Solar Cells. *Electrochim. Acta* **2016**, *200*, 12−20.
(32) Wang, Y.; Fang, H.-B.; Zheng, Y.-Z.; Ye, R.; Tao, X.; Chen, J.-F. Controllable Assembly of Well-Defined Monodisperse Au Nanoparticles on Hierarchical ZnO Microspheres for Enhanced Visible-Light-Driven Photocatalytic and Antibacterial Activity. *Nanoscale* **2015**, *7*, 19118−19128.
(33) Wang, Y.; Zhang, Q.; Huang, F.; Li, Z.; Zheng, Y.-Z.; Tao, X.; Cao, G. In Situ Assembly of Well-Defined Au Nanoparticles in TiO_2 Films for Plasmon-Enhanced Quantum Dot Sensitized Solar Cells. *Nano Energy* **2018**, *44*, 135−143.
(34) Wang, Y.; Fang, H.-B.; Ye, R.-Q.; Zheng, Y.-Z.; Li, N.; Tao, X. Functionalization of ZnO Aggregate Films via Iodine-Doping and TiO_2 Decorating for Enhanced Visible-Light-Driven Photocatalytic Activity and Stability. *RSC Adv.* **2016**, *6*, 24430−24437.
(35) He, Y.; Wang, Y.; Zhang, L.; Teng, B.; Fan, M. High-Efficiency Conversion of CO_2 to Fuel over ZnO/gC_3N_4 Photocatalyst. *Appl. Catal., B* **2015**, *168*, 1−8.
(36) Lu, X.-H.; Zheng, Y.-Z.; Bi, S.-Q.; Zhao, J.-X.; Tao, X.; Chen, J.-F. Enhanced Performance of Dye-Sensitized Solar Cells via the Incorporation of an Internal Layer Consisting of Three-Dimensional Shuttlelike up-Converter and ZnO Nanocrystalline Aggregates. *J. Power Sources* **2013**, *243*, 588−593.
(37) Tian, J.; Zhang, Q.; Uchaker, E.; Gao, R.; Qu, X.; Zhang, S.; Cao, G. Architectured ZnO Photoelectrode for High Efficiency Quantum Dot Sensitized Solar Cells. *Energy Environ. Sci.* **2013**, *6*, 3542−3547.
(38) Huang, F.; Hou, J.; Zhang, Q.; Wang, Y.; Massé, R. C.; Peng, S.; Wang, H.; Liu, J.; Cao, G. Doubling the Power Conversion Efficiency in CdS/CdSe Quantum Dot Sensitized Solar Cells with a ZnSe Passivation Layer. *Nano Energy* **2016**, *26*, 114−122.
(39) Huang, F.; Zhang, L.; Zhang, Q.; Hou, J.; Wang, H.; Wang, H.; Peng, S.; Liu, J.; Cao, G. High Efficiency CdS/CdSe Quantum Dot Sensitized Solar Cells with Two ZnSe Layers. *ACS Appl. Mater. Interfaces* **2016**, *8*, 34482−34489.
(40) Kamat, P. V. Quantum Dot Solar Cells. Semiconductor Nanocrystals as Light Harvesters. *J. Phys. Chem. C* **2008**, *112*, 18737−18753.
(41) Kongkanand, A.; Tvrdy, K.; Takechi, K.; Kuno, M.; Kamat, P. V. Quantum Dot Solar Cells. Tuning Photoresponse Through Size and Shape Control of CdSe-TiO_2 Architecture. *J. Am. Chem. Soc.* **2008**, *130*, 4007−4015.
(42) Yan, K.; Chen, W.; Yang, S. Significantly Enhanced Open Circuit Voltage and Fill Factor of Quantum Dot Sensitized Solar Cells by Linker Seeding Chemical Bath Deposition. *J. Phys. Chem. C* **2013**, *117*, 92−99.
(43) Zhou, R.; Niu, H.; Zhang, Q.; Uchaker, E.; Guo, Z.; Wan, L.; Miao, S.; Xu, J.; Cao, G. Influence of Deposition Strategies on CdSe Quantum Dot-Sensitized Solar Cells: a Comparison Between Successive Ionic Layer Adsorption and Reaction and Chemical Bath Deposition. *J. Mater. Chem. A* **2015**, *3*, 12539−12549.
(44) Yu, X.-Y.; Liao, J.-Y.; Qiu, K.-Q.; Kuang, D.-B.; Su, C.-Y. Dynamic Study of Highly Efficient CdS/CdSe Quantum Dot-Sensitized Solar Cells Fabricated by Electrodeposition. *ACS Nano* **2011**, *5*, 9494−9500.
(45) Bai, S.; Jin, Y.; Liang, X.; Ye, Z.; Wu, Z.; Sun, B.; Ma, Z.; Tang, Z.; Wang, J.; Würfel, U.; et al. Ethanedithiol Treatment of Solution-Processed ZnO Thin Films: Controlling the Intragap States of Electron Transporting Interlayers for Efficient and Stable Inverted Organic Photovoltaics. *Adv. Energy. Mater.* **2015**, *5*, 1401606.
(46) Hou, J.; Zhao, H.; Huang, F.; Jing, Q.; Cao, H.; Wu, Q.; Peng, S.; Cao, G. High Performance of Mn-Doped CdSe Quantum Dot Sensitized Solar Cells Based on the Vertical ZnO Nanorod Arrays. *J. Power Sources* **2016**, *325*, 438−445.
(47) Zheng, Y.-Z.; Zhao, E.-F.; Meng, F.-L.; Lai, X.-S.; Dong, X.-M.; Wu, J.-J.; Tao, X. Iodine-Doped ZnO Nanopillar Arrays for Perovskite Solar Cells with High Efficiency up to 18.24%. *J. Mater. Chem. A* **2017**, *5*, 12416−12425.
(48) Zheng, K.; Karki, K.; Žídek, K.; Pullerits, T. Ultrafast Photoinduced Dynamics in Quantum Dot-Based Systems for Light Harvesting. *Nano Res.* **2015**, *8*, 2125−2142.
(49) Shen, T.; Tian, J.; Lv, L.; Fei, C.; Wang, Y.; Pullerits, T.; Cao, G. Investigation of the Role of Mn Dopant in CdS Quantum Dot Sensitized Solar Cell. *Electrochim. Acta* **2016**, *191*, 62−69.

DOI: 10.1021/acsaem.8b01812
ACS Appl. Energy Mater. 2019, 2, 1259−1265